nature nanotechnology

Article

https://doi.org/10.1038/s41565-022-01308-9

Electrochemically modulated interaction of MXenes with microwaves

Received: 8 August 2022

Accepted: 30 November 2022

Published online: 16 January 2023

Check for updates

Meikang Han[1,2], Danzhen Zhang[1,2], Christopher E. Shuck[1], Bernard McBride[1], Teng Zhang[1], Ruocun (John) Wang[1], Kateryna Shevchuk[1] & Yury Gogotsi[1]

Dynamic control of electromagnetic wave jamming is a notable technological challenge for protecting electronic devices working at gigahertz frequencies. Foam materials can adjust the reflection and absorption of microwaves, enabling a tunable electromagnetic interference shielding capability, but their thickness of several millimetres hinders their application in integrated electronics. Here we show a method for modulating the reflection and absorption of incident electromagnetic waves using various submicrometre-thick MXene thin films. The reversible tunability of electromagnetic interference shielding effectiveness is realized by electrochemically driven ion intercalation and de-intercalation; this results in charge transfer efficiency with different electrolytes, accompanied by expansion and shrinkage of the MXene layer spacing. We finally demonstrate an irreversible electromagnetic interference shielding alertor through electrochemical oxidation of MXene films. In contrast with static electromagnetic interference shielding, our method offers opportunities to achieve active modulation that can adapt to demanding environments.

Dynamic control of interactions between electromagnetic (EM) waves and matter across the visible, infrared and terahertz regions of the EM spectrum has been extensively explored for various applications, such as electrochromic windows, adaptive thermal management, wearable electronics and so on[1–6]. Tuning the response of EM waves with thin films of nanomaterials/nanostructures, aimed at developing highly integrated and adaptive shielding, is of particular interest. This tunability, however, is challenging when the wavelength (λ) of EM waves is much longer than the size scale of nanomaterials, that is, microwaves ($\lambda > 1$ mm).

Electromagnetic interference (EMI) shielding is essential for protecting electronic components against EM jamming, as the number of wireless communication devices, particularly those operating at gigahertz frequencies, in industrial and private spaces has increased by orders of magnitude. Foam materials were developed to mechanically control the reflection and absorption of microwaves, which enables an adjustable EMI shielding capability with deformation[7,8]. However, the thickness of several millimetres hinders the application of porous structures in integrated electronics. To date, thin EMI shielding coatings offer only 'static' protection. Alternatively, electrical control of the interactions between EM waves and materials has been proven effective in optoelectronic and infrared devices[9–12]. Yet, a key feature of current EMI shielding materials is high conductivity, like in conventional metals (Al, Ni, Cu and so on) and carbon materials (graphene, nanotubes, fibres and so on), which leads to reflection of incident EM waves. Generally, the electrical conductivity of metals is not affected by external stimuli. The charge density can be adjusted in graphene through the insertion of ions into the interlayer space but is limited in the microwave range for EMI shielding due to the graphene's inert surface chemistry and electrical double-layer (EDL) charge storage mechanism[13]. Oxidation of graphene quickly decreases its conductivity and EMI shielding capability. Hence, active manipulation of the interaction between centimetre-scale microwaves and thin films remains elusive due to these fundamental challenges at gigahertz frequencies.

MXenes, a large family of two-dimensional (2D) transition metal carbides and nitrides, have emerged as promising EMI shielding materials with a higher shielding effectiveness (SE) than metals and carbons and the ability to produce micrometre-thin free-standing

[1]A. J. Drexel Nanomaterials Institute and Department of Materials Science and Engineering, Drexel University, Philadelphia, PA, USA. [2]These authors contributed equally: Meikang Han, Danzhen Zhang. e-mail: gogotsi@drexel.edu

films[14–17]. The transition metal core layers in MXenes with 2D morphology facilitate electron transport. Moreover, the high conductivity and large redox-active surface of MXenes enable high-rate redox (pseudocapacitive) energy storage with high volumetric capacitance[18–20]. In comparison with EDL capacitors, the surface redox reaction with ion intercalation leads to electron transfer and a change of the surface layer oxidation state accompanied by the change of the interlayer spacing, which further affects the electrical conductivity of MXene electrodes[21–23]. Hence, the combination of metallic conductivity and redox charge storage renders MXenes unique in their response to incident EM waves and offers a possibility to regulate EMI shielding behaviour.

Herein we introduce electrochemically modulated EMI shields made from MXene films with aqueous gel electrolytes (Fig. 1a), which enable reversible modulation of the EMI shielding capability. We systematically performed in situ measurements with different MXenes and electrolytes to verify the effects of the EDL and redox behaviours on the reflection and absorption of EM waves. Furthermore, an electrical 'switch' with a transition from an EMI shielding film to an EM-wave-transparent film is achieved through electrochemical oxidation of MXenes. The demonstrated control of reflection and absorption of centimetre-scale EM waves in the X band (8.2–12.4 GHz) by micrometre-thin MXene films provides a realistic approach towards adaptive EM protection.

Electrochemically modulated EMI shielding with MXenes

The electrochemically modulated EMI shields were assembled with a MXene-coated EM-wave-transparent poly(ethylene terephthalate) (PET) working electrode, a $Ti_3C_2T_x$-coated counter electrode, an electrolyte-containing membrane and a Ag wire as a quasi-reference electrode (Fig. 1a). To track the interactions of the MXene film with the incident EM waves under applied potentials, we selected five common MXenes (V_2CT_x, Ti_2CT_x, $Ti_3C_2T_x$, $V_4C_3T_x$ and $Nb_4C_3T_x$; T_x represents the surface groups). They cover the three typical MXene structures (Fig. 1b and Supplementary Fig. 1) and contain V, Ti and Nb. They cover a broad range of electrical conductivity values (Supplementary Table 1) and have surface redox and EDL electrochemical behaviours in the selected electrolytes[18]. All MXenes were produced through acid etching of the corresponding MAX phases (Supplementary Fig. 2) and consequent delamination (details are provided in the Methods). Typical few-layer flakes after delamination are shown in Supplementary Fig. 3. The delaminated MXene colloidal solutions were spray coated onto the PET substrate to obtain MXene coatings, which were sequentially assembled into shields (Supplementary Fig. 4a–c). To avoid the influence of the highly conductive counter electrode on the scattering (*S*) parameter measurement in the waveguide cavity, a framed $Ti_3C_2T_x$ coating with a blank centre was used (Supplementary Fig. 4b). A 15 × 15 cm^2 flexible MXene-based shield (V_2CT_x working electrode; $Ti_3C_2T_x$ counter electrode) was fabricated to show scalability (Supplementary Fig. 4d). The intercalation of ions into MXene layers was achieved by applying a small potential (under 1 V) to the MXene electrodes (Fig. 1c). Conversely, the ions de-intercalated during discharge, making the operation reversible and cyclic. A cross-sectional scanning electron microscopy (SEM) image of a MXene film shows the well-aligned flakes (Fig. 1d).

EMI shielding was measured in situ on the shields with different MXene electrodes in various electrolytes. The cyclic voltammogram (CV) of the V_2CT_x electrode in 1 M H_2SO_4 gel electrolyte at a scan rate of 3 mV s^{-1} was recorded in a voltage window of 0.8 V (−0.7 to 0.1 V versus Ag wire; Fig. 1e). During the charging process, the EMI SE slightly increases from 23.5 dB to 24.3 dB when the potential changes from 0.1 V to −0.3 V. Remarkably, the EMI SE has a sharp drop from 24.3 dB to 18.1 dB when the potential is increased to −0.7 V, particularly from −0.3 V to −0.5 V. This process corresponds to the pseudocapacitive peaks in the CV, which were ascribed to the oxidation state change of the transition metal around −0.5 V. The EMI SE value returns to its initial value with the discharge process, indicating the reversibility of this feature. Moreover, in contrast to the slow intercalation of ions in other layered materials, even at a high scan rate (50 mV s^{-1}), the EMI shielding change of the V_2CT_x electrode is fast (10 s switching time) and fully reversible, demonstrating the feasibility of instant regulation (Supplementary Video 1). It is possible to develop a shield with a quicker response, considering the outstanding electrochemical performance of MXene at high scan rates[19]. During this charge–discharge process, the change of EMI SE is independent of the frequency (Supplementary Fig. 5a,b), implying a uniform redox reaction and layer spacing change from ion intercalation/de-intercalation. EMI SE values of reflection (SE_R) and absorption (SE_A) show the same trend as the total EMI SE (Supplementary Fig. 5c), unlike when the control of reflection and absorption is done by mechanical deformation of foams[7].

The $Ti_3C_2T_x$ electrode within the same potential window in the protic electrolyte (Fig. 1f), from 0.1 V to −0.4 V, has a notable obvious increase of EMI SE from 35.4 dB to 39.5 dB (by a factor of ~5), implying a substantial increase in the electrical conductivity of the $Ti_3C_2T_x$ film during electrochemical reduction. From −0.4 V to −0.7 V, the EMI SE decreases from 39.5 dB to 36.6 dB, which is similar to the V_2CT_x-based shield and can be explained by the expansion of the interlayer spacing. During the discharge, a symmetric change is observed, corresponding to a pair of coupled redox peaks in the CV. The total EMI SE is also frequency independent (Supplementary Fig. 6a,b) and has the same change with SE_R and SE_A with the applied potential (Supplementary Fig. 6c). Compared with the V_2CT_x shield, $Ti_3C_2T_x$ shows the same two stages of EMI shielding change (an increase followed by a small decrease) but no hysteresis. Similar behaviour can be found in the Ti_2CT_x-based shield (Supplementary Fig. 7a), while there is an almost monotonous change in the $V_4C_3T_x$ (Supplementary Fig. 7c) and $Nb_4C_3T_x$ shields (Supplementary Fig. 7e). These differences are determined by the different electrochemical behaviours of MXenes in different electrolytes, which will be discussed later. V_2CT_x, Ti_2CT_x and $Ti_3C_2T_x$ have obvious redox peaks due to the protonation of surface groups, while only a pair of broad and weak redox peaks appears for $V_4C_3T_x$ and $Nb_4C_3T_x$ in the protic electrolyte[24].

We further investigated the EMI shielding performance of MXenes in a water-in-salt electrolyte (19.8 m LiCl), which was recently demonstrated to provide a desolvation-free Li^+ insertion/deinsertion process for $Ti_3C_2T_x$ MXene under positive potentials[25]. For the V_2CT_x electrode, EMI SE values monotonously increase/decrease in a range of 29.7–31.5 dB with the applied potential between 0.4 and −0.9 V versus Ag wire, and the CV shows a typical EDL charge storage behaviour (Fig. 1g). Ti_2CT_x and $V_4C_3T_x$ electrodes in the water-in-salt electrolyte show a similar trend of EMI SE change because of the EDL charging mechanism (Supplementary Fig. 7b,d). However, for the $Ti_3C_2T_x$ electrode, EMI SE values have a fast drop between 0.2 V and 0 V during charging from 0.6 to −0.8 V. The discharge process shows an opposite trend and an abrupt increase of EMI SE between 0.3 V and 0.5 V (Fig. 1h). These two anomalous changes correspond to a pair of strong peaks at ~0.1 V and ~0.5 V in the CV, which are related to the (de)intercalation of the solvated Li^+ ions, $(Li(H_2O)_3)^+$ accompanied by a large change of the spacing, *d*, between MXene sheets[25].

The mechanism of tunability for reflection and absorption

To understand the fundamental EM wave responses to the electrochemical stimulus, we calculated the reflection and absorption ratios of the incident EM waves for V_2CT_x-based and $Ti_3C_2T_x$-based shields in 1 M H_2SO_4. The reflection ratios of both V_2CT_x and $Ti_3C_2T_x$ show the same trend as the total EMI SE, while the absorption ratios have opposite changes with the applied potentials (Fig. 2a,b). In particular, the maximum gap of the reflection/absorption ratios reaches ~0.1, which is a substantial change at gigahertz frequencies for a thin film. By contrast, the absolute change of reflection/absorption ratios in the $Ti_3C_2T_x$ electrode is slight, which is

https://doi.org/10.1038/s41565-022-01308-9

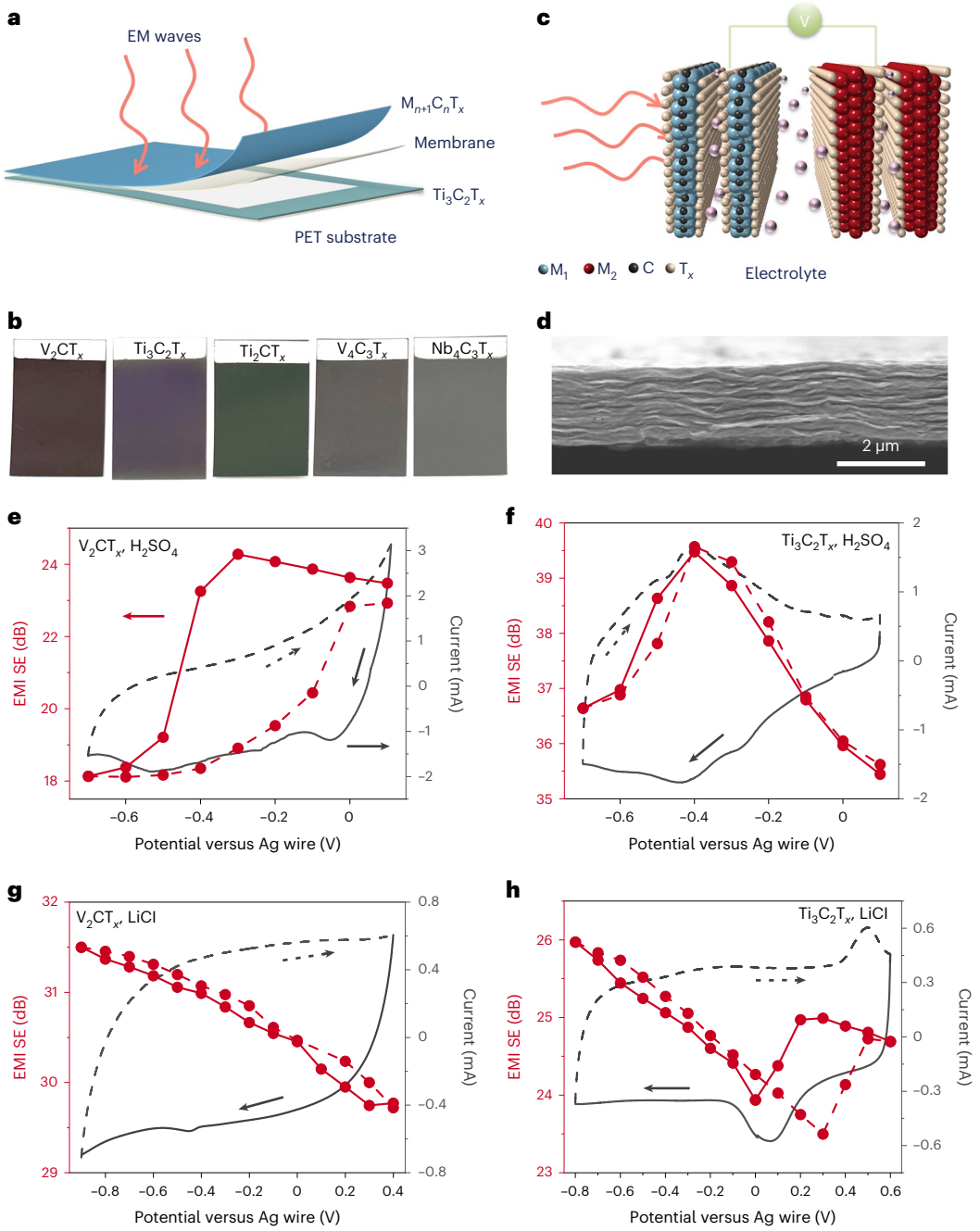

Fig. 1 | Electrochemically modulated EMI shielding behaviours of MXene films. a, Schematic of the shield, which consists of MXene electrodes on a PET substrate and an electrolyte-containing polymer membrane. $M_{n+1}C_nT_x$: M is a transition metal (Ti, V or Nb), C is carbon and T_x is the surface termination. **b**, Digital photos of the MXene electrodes used in this work. **c**, Illustration of ion intercalation between MXene layers for tuning EMI shielding. V, applied voltage. **d**, SEM image of the cross-section of a MXene film, showing the aligned layers. **e**–**h**, Potential-dependent EMI SE and the CVs of the device using a V_2CT_x electrode in 1 M H_2SO_4 (**e**), $Ti_3C_2T_x$ electrode in 1 M H_2SO_4 (**f**), V_2CT_x electrode in 19.8 m LiCl (**g**), and $Ti_3C_2T_x$ electrode in 19.8 m LiCl (**h**), showing the bidirectional tunability of EMI SE with different MXenes in different electrolytes.

distinct from the EMI SE values. This is dictated by the electrode's high electrical conductivity (>10,000 S cm^{-1}), which accounts for the domination of reflection (>90%). In other words, moderate conductivity can lead to a larger modulation of the reflection/absorption ratio. Considering a wide range of electrical conductivities and surface compositions of MXenes[26], the control of reflection/absorption in MXenes can certainly be further optimized for practical applications.

For further insights into the relationship between EM response and electrochemical reactions, we performed in situ X-ray diffraction and Raman spectroscopy measurements for $Ti_3C_2T_x$-based shields during cyclic voltammetry. When $Ti_3C_2T_x$ in 1 M H_2SO_4 was charged, the *d* spacing decreased from 13.75 Å to 13.54 Å from 0.1 V to −0.3 V and then increased to 14.01 Å between −0.3 V and −0.7 V (Fig. 2c and Supplementary Fig. 8a). The discharge process shows a reversible *d* spacing change. We also recorded microscopic shrinkage and expansion of the V_2CT_x electrode during charge and discharge using laser scanning confocal microscopy (Supplementary Video 2). The focus shift where the blurry image turns clear indicates film expansion. This demonstrates that EMI SE increases with the shrinkage of the MXene film and decreases with its expansion upon protonation/deprotonation[27]. Raman spectra show a shift of the A_{1g} (C) peak, which is assigned to out-of-plane vibrations of carbon, especially with an applied potential

https://doi.org/10.1038/s41565-022-01308-9

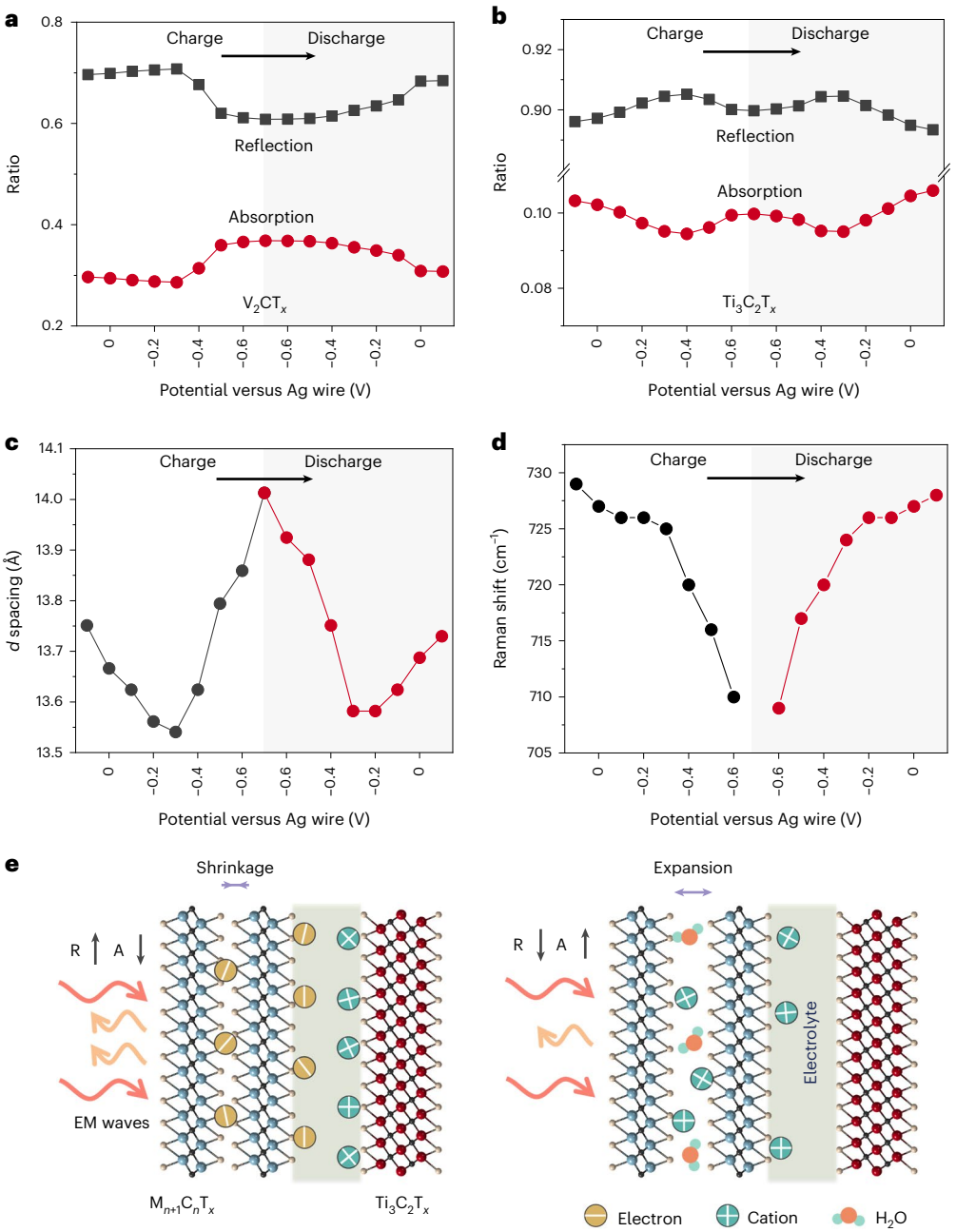

Fig. 2 | Electrochemical control of the reflection and absorption of microwaves, and the mechanism of bidirectional tunability. a,**b**, Potential dependence of the reflection and absorption ratios versus applied potential recorded using a V_2CT_x electrode in 1 M H_2SO_4 (**a**) and a $Ti_3C_2T_x$ electrode in 1 M H_2SO_4 (**b**). **c**,**d**, In situ X-ray diffraction and Raman spectra showing variations of the *d* spacing (**c**) and Raman shift (**d**) of the A_{1g} (C) peak of the $Ti_3C_2T_x$ electrode in 1 M H_2SO_4. **e**, Illustration of the mechanisms for electrochemically modulated EMI shielding: the charge transfer resulting from electrosorption of ions, M element oxidation state change and layer spacing change between MXene sheets. R is reflection, and A is absorption.

from −0.3 V to −0.7 V (Fig. 2d and Supplementary Fig. 8a)[28]. In agreement with the change of *d* spacing, a drastic peak shift starts at −0.3 V, which is ascribed to the oxidation state change of titanium. Similarly, for the $Ti_3C_2T_x$ electrode in 19.8 m LiCl, the A_{1g} (C) peak downshifts from ~728 cm^{-1} to ~720 cm^{-1} upon charging (Supplementary Fig. 9). Larger peak shifts occur at ~0.2 V (charge) and ~0.3 V (discharge), which correspond to the pair of peaks in the electrode's CV.

According to the above in situ analysis, we propose interaction mechanisms of MXene films with incident microwaves based on the distinct electrochemical behaviours (Fig. 2e). First, in the case of the EDL process, the intercalation of cations between negatively charged MXene layers under an applied potential reduces the interlayer spacing due to the increased electrostatic attraction, which leads to an increase in electrical conductivity and EMI SE. Second, the insertion of partially desolvated cations between MXene sheets occurring in water-in-salt electrolytes results in a decrease of EMI SE with the increase of *d* spacing. Third, the redox behaviour in MXenes continuously changes the oxidation state of the transition metal on charge–discharge and thereby gives rise to the expansion of the interlayer spacing and a change in surface chemistry and film conductivity. Thus, the decreased EMI SE accompanied by the increase in absorption is achieved as a consequence of a decrease in conductivity. Since electrolyte confinement changes with applied potentials, there is a continuous transition between EDL capacitance and Faradaic intercalation (surface redox)[21].

https://doi.org/10.1038/s41565-022-01308-9

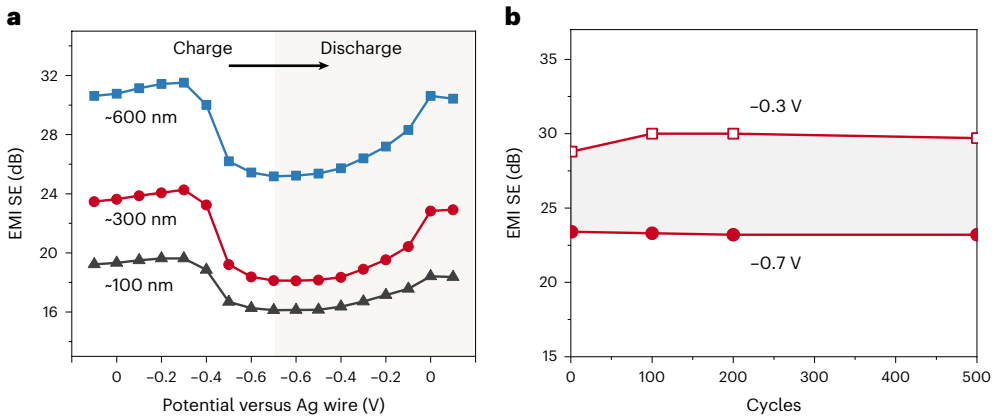

Fig. 3 | Thickness-dependent behaviour and cycling stability. a, Thickness-dependent EMI SE as a function of applied potential, showing the increasing change of EMI SE with increasing thickness. **b**, Cycling stability of the device with the V_2CT_x electrode in 1 M H_2SO_4, showing the steady performance over 500 cycles.

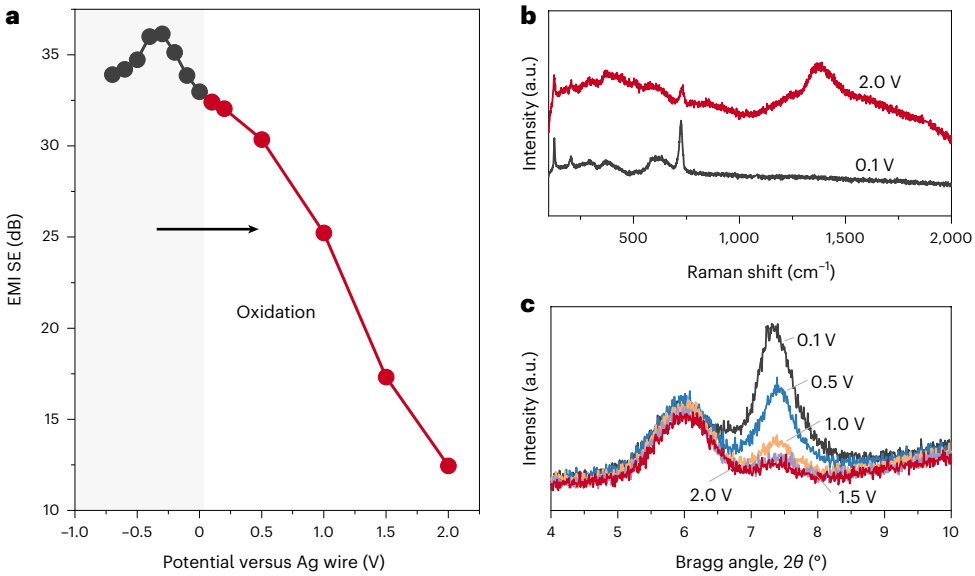

Fig. 4 | An EMI shielding 'switch' with MXene. a, Potential-dependent EMI SE of the $Ti_3C_2T_x$ electrode in 1 M H_2SO_4, showing the decrease in electromagnetic protection by about 350 times from 0.1 V to 2 V. **b**,**c**, In situ Raman (**b**) and X-ray diffraction (**c**) analyses of the film oxidation process, demonstrating the switch mechanism.

This feature facilitates the fast directional modulation of reflection and absorption in MXene films upon charge–discharge.

Thickness-dependent behaviour and cycling stability

Given the importance of the ion confinement between MXene layers and the notable change of EMI SE for the V_2CT_x electrode, we investigated the effect of film thickness on changes in the EMI shielding of V_2CT_x in 1 M H_2SO_4 (Fig. 3a). The EMI SE of all films increases with increasing thickness from ~100 nm to ~600 nm, and the same trend is observed for the EMI SE change with the applied potential, independent of the thickness. However, the variation amplitude of EMI SE increases when the film is thicker. For example, the difference between the maximum value (31.5 dB at −0.3 V) and the minimum value (25.2 dB at −0.7 V) for the ~600 nm film is 6.3 dB compared to 3.5 dB for an ~100-nm-thick V_2CT_x electrode. This demonstrates that the number of MXene layers notably influences our ability to control the EM wave response due to the varying degrees of intercalation and film property changes. However, the excessive film thickness may lead to a strong reflection, which weakens the change of EMI SE. The long-term stability of the V_2CT_x device in 1 M H_2SO_4 was evaluated by in situ EMI measurement with cyclic voltammetry at 20 mV s^{-1}. This shows that the device operates steadily after 500 cycles with almost unchanged CVs and has a stable and reversible change of EMI SE (Fig. 3b and Supplementary Fig. 10a,b) during charge–discharge. The $Ti_3C_2T_x$ shield in 1 M H_2SO_4 was also stable for over 500 cycles, in agreement with its electrochemical stability (Supplementary Fig. 10c,d).

MXene-based EMI shielding 'alertor'

We further applied positive potentials to the $Ti_3C_2T_x$ shields in aqueous electrolytes to investigate their EM wave response to the anodic oxidation of MXene. When the positive potential exceeds 0.1 V versus Ag wire, the EMI SE value of the $Ti_3C_2T_x$ electrode in 1 M H_2SO_4 shows a fast and continuous drop from 32.98 dB (0.1 V) to 12.45 dB (2.0 V; Fig. 4a). Moreover, the trends of EMI SE values with increasing frequency become different (Supplementary Fig. 11a), which may be ascribed to EM wave scattering from nonuniform oxidation of the $Ti_3C_2T_x$ film. Notably, the average ratios of absorption, reflection and transmission of the device at 2.0 V were 0.49, 0.43 and 0.08, respectively, while the ratios of absorption and reflection at 0.1 V were 0.23 and 0.77, and the transmission was negligible. Raman spectra show that the relative intensity of the A_{1g} (C) peak at ~723 cm^{-1} decreases and a broad peak appears

at around 1,378 cm^{-1} (Fig. 4b), when the applied potential is 2.0 V. This is due to the formation of amorphous carbon upon the surface oxidation of $Ti_3C_2T_x$ (ref. 29). X-ray diffraction patterns recorded in situ show two broad peaks at ~6.0° and ~7.3°, which are assigned to the $Ti_3C_2T_x$ counter electrode and the working electrode, respectively (Fig. 4c). Notably, the peak intensity of the working electrode decreased with the applied potentials whereas no obvious change could be observed for the counter electrode. This indicates that the degree of disorder of stacked $Ti_3C_2T_x$ sheets increases during the oxidation process under positive potentials. The oxidation of the $Ti_3C_2T_x$ electrode in 19.8 m LiCl shows a similar phenomenon where the EMI SE value decreases from 22.33 dB (0.6 V) to 14.28 dB (1.5 V; Supplementary Fig. 12). These results indicate that the MXene films can convert from EMI shielding to quasi-EM wave transmission by electrochemical oxidation of the MXenes. The MXene film can potentially serve as a dynamic EMI shielding switch, although the oxidation process is irreversible. The application of a small voltage can unseal the protected electronic device and allow communication with it. This MXene-based 'alertor' can protect electronic devices from undesired access or damage during transportation and storage. Furthermore, the sensitivity of the shields can be tuned for specific scenarios by controlling the anodic oxidation of different MXene compositions in different electrolytes.

The correlation between the electrochemical behaviour of MXenes and their interaction with EM radiation needs more profound understanding, given that the MXene family offers a large variety of compositions, structures and surface groups[30]. Moreover, the size and arrangement of MXene flakes could also affect their electrochemical performance. This means that the control of the EM wave response at gigahertz frequencies can be further optimized by modification of MXenes and confined electrolytes. The combination of varied electrical conductivities and redox-active transition metal atoms makes electrochemically modulated MXene shields promising for fundamental studies aimed at understanding the interaction of nanometre-scale MXene sheets with centimetre-scale EM waves[31]. This combination of properties is also of great potential for the adaptive EM protection of electronics in practice[32]. For example, for electronic devices overheating the shield after a long time running or operating in extreme environments, the EMI shielding performance can be controlled with tunable MXene shields. Also, object identification can be achieved with the detection of active MXene shields that have varied EM signals, especially for the highly integrated system. Furthermore, we envision that our concept can be combined with metasurfaces by patterning MXene electrodes to achieve precise local control of the reflection, absorption and transmission of microwaves in thin films, which could be an exciting direction to explore.

Conclusions

In summary, we have demonstrated electrochemically modulated MXene shields, which can modulate the response to incident EM waves and EMI shielding effectiveness at gigahertz frequencies. Bidirectional tunability of the EMI SE is achieved with a continuous transition from the EDL to redox charge storage in MXene electrode films with aqueous electrolytes. Particularly, the surface redox processes in MXene electrodes, accompanied by a change in the oxidation state of the transition metal, ion intercalation and interlayer spacing expansion/contraction, change the ratio of absorption to reflection and the total EMI SE. An EMI shielding switch has been designed by using the anodic oxidation of MXenes. Our results offer insight into the fundamental understanding of the interactions of microwaves with thin films and build a platform for developing adaptive EMI shields with dynamic regulation.

Online content

Any methods, additional references, Nature Portfolio reporting summaries, source data, extended data, supplementary information, acknowledgements, peer review information; details of author contributions and competing interests; and statements of data and code availability are available at https://doi.org/10.1038/s41565-022-01308-9.

References

1. Ergoktas, M. S. et al. Multispectral graphene-based electro-optical surfaces with reversible tunability from visible to microwave wavelengths. *Nat. Photon.* **15**, 493–498 (2021).
2. Zhang, X. A. et al. Dynamic gating of infrared radiation in a textile. *Science* **363**, 619–623 (2019).
3. Ergoktas, M. S. et al. Topological engineering of terahertz light using electrically tunable exceptional point singularities. *Science* **376**, 184–188 (2022).
4. Peng, J. et al. Scalable electrochromic nanopixels using plasmonics. *Sci. Adv.* **5**, eaaw2205 (2019).
5. Xu, J., Mandal, J. & Raman, A. P. Broadband directional control of thermal emission. *Science* **372**, 393–397 (2021).
6. Dyachenko, P. N. et al. Controlling thermal emission with refractory epsilon-near-zero metamaterials via topological transitions. *Nat. Commun.* **7**, 11809 (2016).
7. Han, M. et al. Anisotropic MXene aerogels with a mechanically tunable ratio of electromagnetic wave reflection to absorption. *Adv. Opt. Mater.* **7**, 1900267 (2019).
8. Qiu, L., Li, D. & Cheng, H.-M. Structural control of graphene-based materials for unprecedented performance. *ACS Nano* **12**, 5085–5092 (2018).
9. Liu, W. et al. Graphene charge-injection photodetectors. *Nat. Electron.* **5**, 281–288 (2022).
10. Inoue, T., De Zoysa, M., Asano, T. & Noda, S. Realization of dynamic thermal emission control. *Nat. Mater.* **13**, 928–931 (2014).
11. Low, T. et al. Polaritons in layered two-dimensional materials. *Nat. Mater.* **16**, 182–194 (2017).
12. Fang, Y., Ge, Y., Wang, C. & Zhang, H. Mid-infrared photonics using 2D materials: status and challenges. *Laser Photon. Rev.* **14**, 1900098 (2020).
13. Balci, O., Polat, E. O., Kakenov, N. & Kocabas, C. Graphene-enabled electrically switchable radar-absorbing surfaces. *Nat. Commun.* **6**, 6628 (2015).
14. VahidMohammadi, A., Rosen, J. & Gogotsi, Y. The world of two-dimensional carbides and nitrides (MXenes). *Science* **372**, eabf1581 (2021).
15. Shahzad, F. et al. Electromagnetic interference shielding with 2D transition metal carbides (MXenes). *Science* **353**, 1137–1140 (2016).
16. Iqbal, A. et al. Anomalous absorption of electromagnetic waves by 2D transition metal carbonitride Ti_3CNT_x (MXene). *Science* **369**, 446–450 (2020).
17. Kamysbayev, V. et al. Covalent surface modifications and superconductivity of two-dimensional metal carbide MXenes. *Science* **369**, 979–983 (2020).
18. Anasori, B., Lukatskaya, M. R. & Gogotsi, Y. 2D metal carbides and nitrides (MXenes) for energy storage. *Nat. Rev. Mater.* **2**, 16098 (2017).
19. Lukatskaya, M. R. et al. Ultra-high-rate pseudocapacitive energy storage in two-dimensional transition metal carbides. *Nat. Energy* **2**, 17105 (2017).
20. VahidMohammadi, A., Mojtabavi, M., Caffrey, N. M., Wanunu, M. & Beidaghi, M. Assembling 2D MXenes into highly stable pseudocapacitive electrodes with high power and energy densities. *Adv. Mater.* **31**, 1806931 (2019).
21. Fleischmann, S. et al. Continuous transition from double-layer to Faradaic charge storage in confined electrolytes. *Nat. Energy* **7**, 222–228 (2022).
22. Wang, X. et al. Surface redox pseudocapacitance of partially oxidized titanium carbide MXene in water-in-salt electrolyte. *ACS Energy Lett.* **7**, 30–35 (2021).

23. Simon, P. & Gogotsi, Y. Perspectives for electrochemical capacitors and related devices. *Nat. Mater.* **19**, 1151–1163 (2020).
24. Zhao, S. et al. Flexible $Nb_4C_3T_x$ film with large interlayer spacing for high-performance supercapacitors. *Adv. Func. Mater.* **30**, 2000815 (2020).
25. Wang, X. et al. Titanium carbide MXene shows an electrochemical anomaly in water-in-salt electrolytes. *ACS Nano* **15**, 15274–15284 (2021).
26. Han, M. et al. Beyond $Ti_3C_2T_x$: MXenes for electromagnetic interference shielding. *ACS Nano* **14**, 5008–5016 (2020).
27. Mu, X. et al. Revealing the pseudo-intercalation charge storage mechanism of MXenes in acidic electrolyte. *Adv. Func. Mater.* **29**, 1902953 (2019).
28. Sarycheva, A. & Gogotsi, Y. Raman spectroscopy analysis of the structure and surface chemistry of $Ti_3C_2T_x$ MXene. *Chem. Mater.* **32**, 3480–3488 (2020).
29. Tang, J. et al. Tuning the electrochemical performance of titanium carbide MXene by controllable in situ anodic oxidation. *Angew. Chem. Int. Ed.* **131**, 18013–18019 (2019).
30. Gogotsi, Y. & Anasori, B. The rise of MXenes. *ACS Nano* **13**, 8491–8494 (2019).
31. Che, R. C., Peng, L. M., Duan, X. F., Chen, Q. & Liang, X. L. Microwave absorption enhancement and complex permittivity and permeability of Fe encapsulated within carbon nanotubes. *Adv. Mater.* **16**, 401–405 (2004).
32. Sun, H. et al. Cross-stacking aligned carbon-nanotube films to tune microwave absorption frequencies and increase absorption intensities. *Adv. Mater.* **26**, 8120–8125 (2014).

Methods

Materials

For the synthesis of the MAX phases, Ti (99.5%, Alfa Aesar), V (99.5%, Alfa Aesar), Nb (99.99%, Beantown Chemical), Al (99.5%, Alfa Aesar), graphite (99%, Alfa Aesar) and TiC (99.5%, Alfa Aesar) powders were used.

For the topochemical synthesis of MXenes, hydrofluoric acid (HF, 48.5–51%, Acros Organics), hydrochloric acid (HCl, 36.5–38%, Fisher Chemical), lithium chloride (LiCl, 99%, Acros Organics), lithium fluoride (LiF, 98.5%, Alfa Aesar) and tetramethylammonium hydroxide (TMAOH, 25 wt%, Acros Organics) were used.

For the fabrication of the shields, sulfuric acid (H_2SO_4, 98%, Fisher Chemical), polyvinyl alcohol (PVA, Alfa Aesar) and PET (100 µm thick, TruLam) were used.

Synthesis of MAX phases

Prior to synthesis, all precursor powders (Table 1) were weighed and then ball-milled with zirconia balls for 18 h. The powder mixture was then transferred to alumina crucibles, which were placed into a high-temperature furnace. Argon was flowed through the furnace for 1 h before heating, then was kept flowing through the furnace during synthesis. The heating rate was 3 °C min^{-1}. Depending on the chemistry and composition, different temperatures and annealing times were used (details in Table 1). After cooling, the samples were milled and then sieved to <75 µm.

Synthesis of $Ti_3C_2T_x$ and Ti_2CT_x

$Ti_3C_2T_x$ and Ti_2CT_x were synthesized by etching the corresponding MAX phase powders (Ti_3AlC_2 and Ti_2AlC) with HF and HCl. Typically, 12 ml of HCl, 2 ml of HF and 6 ml of deionized (DI) water were mixed with stirring first. After that, 1 g of MAX powder was gradually added to the mixed solution and it continued to be stirred for 24 h at room temperature. After the etching was done, the reacted solution was washed by centrifugation at 2,550*g* for 2 min. This washing process was repeated until the pH value was >6. The centrifuged sediment was added to a solution of LiCl (1 g) in DI water (50 ml). The mixture was shaken for 30 min at room temperature. After that, the solution was washed by centrifugation at 2,550*g* for 10 min. The centrifugation was repeated until the pH value was >6. After the sediment swelled, the solution was finally centrifuged at 7,230*g* for 3 min. The supernatant was used for the preparation of MXene electrodes.

Synthesis of V_2CT_x, $V_4C_3T_x$ and $Nb_4C_3T_x$

V_2CT_x, $V_4C_3T_x$ and $Nb_4C_3T_x$ were synthesized by etching the corresponding MAX phases (V_2AlC, V_4AlC_3 and Nb_4AlC_3) with HF. Typically, 1 g of V_2AlC powder was added to 20 ml of HF. The mixture was stirred at 35 °C for 48 h. After etching, the reacted solution was repeatedly washed with DI water through centrifugation at 2,550*g* for 2 min until the pH was >6. After washing, the sediment was dispersed in a mixture of 10 ml DI water and 0.5 g TMAOH and then stirred for 24 h. After that, the mixture was washed repeatedly with DI water by centrifugation at 12,850*g* for 10 min until the pH was <8. At last, the supernatant was collected after centrifugation at 2,550*g* for 10 min. For V_4AlC_3 and $Nb_4C_3T_x$, the etching and delamination procedures were similar to those of V_2CT_x, except the etching time was seven days and the delamination time was 48 h.

Fabrication of MXene shields

MXene films were fabricated by a spray-coating method. First, a PET sheet was cut into 4.5 cm × 3 cm pieces and cleaned by bath sonication (Branson 2510 Ultrasonic Cleaner, 100 W) in DI water for 15 min and then dried with compressed air. The cleaned PET pieces were plasma treated (Tergeo Plus, Pie Scientific) at 100 W with Ar/O_2 (3/5 sccm) for 5 min to make the surface hydrophilic. The pretreated pieces were spray coated using a manual spray gun filled with dilute MXene colloidal solution in water (1–2 mg ml^{-1}) at room temperature. To accelerate drying and ensure a uniform surface, a hair dryer was used to dry each sprayed layer. For the spray-coating process of the counter electrode, a square mask (2.5 cm × 1.2 cm) was applied to the middle of a PET piece to get a framed $Ti_3C_2T_x$ coating. After spray coating, MXene films were dried in a vacuum oven overnight before performing experiments.

EMI shields were fabricated using different MXene films as working electrodes, silver wire as a reference electrode and $Ti_3C_2T_x$ films with a blank region in the middle as counter electrodes. Electrolyte-containing membrane (MCE Membrane, Thermal Scientific, 0.22 µm pore size) was used as a separator between electrodes. A copper foil was used to connect the electrodes and potentiostat. The acidic electrolyte was fabricated by mixing 10 ml 1 M H_2SO_4 and 0.5 g PVA with stirring at 80 °C for 12 h. The water-in-salt electrolyte was fabricated by mixing 10 ml 19.8 m LiCl and 0.5 g PVA with stirring at 80 °C for 12 h.

Table 1 | The synthesis conditions of the MAX phases used in this work

Type	MAX phase	Precursors	Atomic ratio	Annealing temperature (°C)	Annealing time (h)
211	Ti_2AlC	Ti/Al/C	2:1.1:0.9	1,550	2
	V_2AlC	V/Al/C	2:1.1:0.9	1,550	2
312	Ti_3AlC_2	TiC/Al/Ti	2:2.2:1.25	1,380	2
413	Nb_4AlC_3	Nb/Al/C	4:1.1:2.7	1,650	4
	V_4AlC_3	V/Al/C	4:1.5:3	1,500	2

Characterization

X-ray diffraction patterns of MAX phases and MXene films were measured using a Rigaku SmartLab operating at 40 kV/30 mA with Cu Kα radiation. Raman measurement was carried out with an inverted reflection mode Renishaw (inVia) instrument, equipped with ×63 (numerical aperture, 0.7) objectives and a diffraction-based room-temperature spectrometer. The laser wavelength was 785 nm, the acquisition time was 40 s and the laser power was kept around 0.1 mW. Three-dimensional laser scanning confocal microscopy (Keyence, VK-X1000) was used to observe the surface of MXene electrodes and measure the thickness. The cross-section of the MXene film was observed using SEM (Zeiss Supra 50VP). The electrical conductivity of MXene films was measured using a four-point probe instrument (ResTest, Jandel Engineering), with a probe distance of 1 mm. An average value was taken from three different locations on the film. The in situ Raman and X-ray diffraction measurements were carried out using the multiple potential step chronoamperometry method. The electrochemical tests were conducted at room temperature using a BioLogic SP 150 potentiostat.

A vector network analyser (8720ES, Agilent) with a WR-90 rectangular waveguide in the frequency range of 8.2–12.4 GHz was used to measure the *S* parameters of MXene shields during the CV scanning at 3 mV s^{-1}. The shield was mounted onto the sample holder and then tightly fixed with clamps.

The EMI SE was calculated based on the *S* parameters (S_{11} and S_{21}). The transmission power (T; $T = |S_{21}|^2$), reflectivity power (R; $R = |S_{11}|^2$) and absorption power (A) are related as $A + R + T = 1$. The total EMI shielding effectiveness (SE_{total}), reflection effectiveness (SE_R) and absorption effectiveness (SE_A) associated with the incident wave and transmitted wave are calculated as follows:

$$SE_{total} = 10\log_{10}\left(\frac{1}{T}\right) \quad (1)$$

$$SE_R = 10\log_{10}\left(\frac{1}{1-R}\right) \quad (2)$$

$$SE_A = 10\log_{10}\left(\frac{1-R}{T}\right) \quad (3)$$

Data availability

All relevant data are available from the authors on reasonable request, and/or are included within the manuscript and its Supplementary Information. Source data are provided with this paper.

Acknowledgements

This work was supported by the US National Science Foundation (grants ECCS-2034114 and DMR-2041050; Y.G.) and Murata Manufacturing (Japan). X-ray diffraction analysis was performed using instruments in the Materials Characterization Core at Drexel University.

Author contributions

M.H. and Y.G. conceived this study. M.H. and D.Z. designed and performed the shield testing. M.H., D.Z. and B.M. synthesized the MXenes and fabricated the MXene films. C.E.S. synthesized the MAX phases. C.E.S. and D.Z. performed the X-ray diffraction measurements. T.Z. performed the SEM observation. D.Z., R.(J.)W. and K.S. contributed to the Raman investigations. M.H. wrote the manuscript with input from all coauthors under supervision from Y.G.

Competing interests

The work is subjected to a patent application (#63/366,852) by M.H., Y.G. and D.Z. The authors declare no other competing interests.

Additional information

Supplementary information The online version contains supplementary material available at https://doi.org/10.1038/s41565-022-01308-9.

Correspondence and requests for materials should be addressed to Yury Gogotsi.

Peer review information *Nature Nanotechnology* thanks Majid Beidaghi and the other, anonymous, reviewer(s) for their contribution to the peer review of this work.